Liquid Crystals
Publication details, including instructions for authors and subscription information:
http://www.informaworld.com/smpp/title~content=t713926090

New ferroelectric liquid crystalline materials with an azo group in the molecular core

Miroslav Kašpar[a]; Alexej Bubnov Corresponding author[a]; Věra Hamplová[a]; Slavomír Pirkl[b]; Milada Glogarová[a]
[a] Institute of Physics, Academy of Sciences of the Czech Republic, 182 21 Prague 8, Czech Republic [b] University of Pardubice, 532 10 Pardubice, Czech Republic

Online publication date: 25 May 2010

To cite this Article Kašpar, Miroslav , Bubnov Corresponding author, Alexej , Hamplová, Věra , Pirkl, Slavomír and Glogarová, Milada(2004) 'New ferroelectric liquid crystalline materials with an azo group in the molecular core', Liquid Crystals, 31: 6, 821 — 830
To link to this Article: DOI: 10.1080/02678290410001697567
URL: http://dx.doi.org/10.1080/02678290410001697567

LIQUID CRYSTALS, 2004, VOL. 31, NO. 6, 821–830

New ferroelectric liquid crystalline materials with an azo group in the molecular core

MIROSLAV KAŠPAR, ALEXEJ BUBNOV*, VĚRA HAMPLOVÁ, SLAVOMÍR PIRKL† and MILADA GLOGAROVÁ

Institute of Physics, Academy of Sciences of the Czech Republic, Na Slovance 2, 182 21 Prague 8, Czech Republic
†University of Pardubice, Studentská 95, 532 10 Pardubice, Czech Republic

(*Received 4 August 2003; in final form 20 January 2004; accepted 9 February 2004*)

Six series of new liquid crystalline materials with an azo group (N=N) located in different parts of the mesogenic core of the molecule have been synthesized and their physical properties studied. The chiral segments of these materials are based on alkoxypropionate or alkyllactate units. It has been found that lateral methyl substitution on a phenyl ring in the molecular core disturbs the packing of the molecules. As a result smectic phases disappear and the phase transition temperatures decrease. In addition, shifting the N=N group closer to the chiral centre of the molecule leads to the disappearance of the ferroelectric SmC* phase. For the compounds which show the ferroelectric SmC* phase, the temperature dependence of the spontaneous polarization, the spontaneous tilt angle, the helix pitch length and the complex permittivity has been studied. The effect of shifting the azo group in the molecular core on the physical properties is discussed.

1. Introduction

Liquid crystalline materials, either low molar mass or polymeric in nature, containing an azo group in the mesogenic core, are often studied from the point of view of their interesting optical properties, which enable application in, for example, optical switching, holography and optical storage devices [1–6]. In addition, grafted polysiloxanes with mesogens containing azobenzene have been successfully prepared possessing excellent properties namely, perfect transparency, high oxidation stability and good thermal stability [7, 8]. In most cases, these compounds were achiral forming mainly smectic C (SmC) and nematic (N) phases.

Relatively few chiral azo compounds have been studied to date and most of these are based on the commercially available chiral 2-methylbutanol [9] and 2-octanol [10, 11] units. The antiferroelectric phase occurred in some of these materials, probably, due to the presence of the 2-octyl group. Azo compounds laterally substituted by fluorine, and in which the chiral part was based on the 2-octyl group connected to the mesogenic core by an ether link, have also been studied [12]. These compounds show the chiral ferroelectric smectic (SmC*) phase, the cholesteric (N*) phase and the blue phase (BP). The paraelectric smectic A (SmA) phase was not found; similar behaviour was seen for chlorine-substituted compounds [13]. A ferroelectric liquid crystalline compound with the commercial ethyllactate as the chiral fragment was prepared and used as a mesogenic side group in grafted polysiloxanes [14].

For potential commercial applications the existence of mesophases at lower temperatures is of very high importance. Lateral substitution by a methyl group used for some of these azo compounds was chosen for the expected influence of this substituent is to decrease the phase transition temperatures [15].

In recent years we have systematically studied different types of liquid crystalline compounds containing a chiral segment derived from (*S*)-lactic acid. In this study we have focused on the effect of the azo group, introduced into different locations on the mesogenic core of the molecule, on the mesomorphic and physical properties of non-substituted or laterally methyl-substituted liquid crystals with alkoxypropionate or alkyllactate as the chiral unit. The general formulae of materials studied here are shown in scheme 1.

2. Synthesis

The general procedure for the preparation of the **Ia** ***m/n*** and **Ib** ***m/n*** homologues is shown in scheme 2. 4-Alkoxy-4′-hydroxyazobenzenes **2** were obtained from 4-acetamidophenol **1** using standard methods of

*Author for correspondence; e-mail: bubnov@fzu.cz

Liquid Crystals ISSN 0267-8292 print/ISSN 1366-5855 online © 2004 Taylor & Francis Ltd
http://www.tandf.co.uk/journals
DOI: 10.1080/02678290410001697567

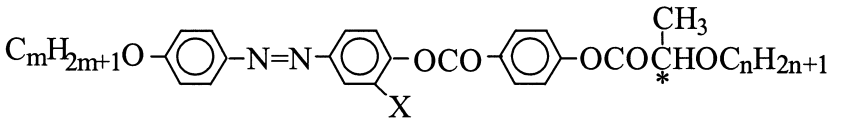

Ia *m/n*: *X* = CH_3
Ib *m/n*: *X* = H

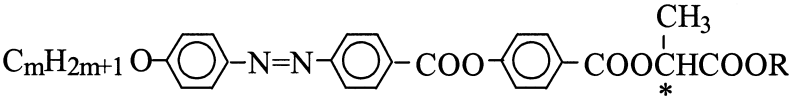

II *m/n*: *R* = C_nH_{2n+1}
II *m/: *R* = $CH_2CH^*(CH_3)CH_2CH_3$**

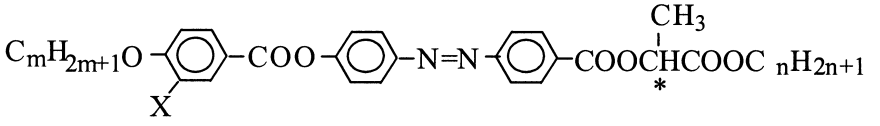

IIIa *m/n*: *X* = CH_3
IIIb *m/n*: *X* = H

Scheme 1.

alkylation, diazotation and coupling (using phenol or *o*-cresol) [16]. Mesogenic phenols **3** were obtained by esterification of **2** with 4-methoxycarbonyloxybenzoic acid chloride in dry pyridine followed by ammonolysis by 30% ammonia solution at room temperature for 3 h in a mixture of ethanol and acetone (1/1). The solution was then poured into 5% HCl in water and cooled in a refrigerator. The precipitated yellow product was recrystallized from a mixture of ethanol and tetrahydrofurane (3/1). Dry mesogenic phenols were esterified with the appropriate alkoxypropionic acids in the presence of dicyclohexylcarbodiimide (DCC) and dimethylaminopyridine (DMAP) as a catalyst yielding the final products **Ia *m/n*** and **Ib *m/n*** ^{1}H NMR ($CDCl_3$, 200 MHz) for **Ia 4/8** δ (ppm): 8.28 (2H, d, $J=8.2$, *ortho* to –COO); 7.80 (2H, m, *ortho* and *para* to $-CH_3$); 7.90 (2H, d, $J=9.3$, *ortho* to –N=N–); 7.28 (3H, m, *ortho* to –OCO); 7.00 (2H, d, $J=8.8$, *ortho* to *R*O–); 4.22 (1H, q, $J=6.8$, C*H); 4.04 (2H, t, $J=6.6$, CH_2OAr); 3.50 and 3.70 (1+1H, m, $\underline{CH_2}OC^*$); 2.32 (3H, s, CH_3Ar); 1.81 (2H, quint, $J=7.4$, $\underline{CH_2}CH_2OAr$); 1.64 (2H, quint., $J=7.2$, $\underline{CH_2}$ CH_2OC^*); 1.60 (3H, d, $J=7{,}0$, CH_3C^*); 1.20–1.60 (12H, m, CH_2); 1.00 (3H, t, $J=7.4$, CH_3 in *m*-chain); 0.90 (3H, t, $J=6.3$, CH_3 in *n*-chain).

In scheme 3, the general procedure for the preparation of the **II *m/n*** and **II *m/**** homologues is presented. All 4-alkoxyazobenzene-4′-carboxylic acids **5** were obtained from 4-aminobenzoic acid by diazotation and coupling with phenol. The problematic alkylation of acid **4** was realized with good yield in dimethylformamide with 2 mol of sodium hydride at 100°C for several hours. Ethyl alcohol and KOH solution was then added to the mixture which was heated under reflux with stirring for 1 h to destroy the ester. The mixture was poured into water, acidified by HCl and the orange precipitate separated and washed with water. The product of reaction with alkyl-2-(4-hydroxybenzoyloxy)propionate [17] yielded yellow crystals of final products **II *m/**** and **II *m/n***. ^{1}H NMR ($CDCl_3$, 200 MHz) for **II 8/6** δ (ppm): 8.33 (2H, d, $J=8.2$, *ortho* to –COOAr); 8.18 (2H, d, $J=8.2$, *ortho* to –COOC*); 7.95 (4H, m, *ortho* to –N=N–); 7.35 (2H, d, $J=8.2$, *ortho* to –OCOAr); 7.02 (2H, d, $J=8.8$, *ortho* to *R*O–); 5.34 (1H, q, $J=7.4$, C*H); 4.18 (2H, m, CH_2OCOC^*); 4.04 (2H, t, $J=6.6$, CH_2OAr); 1.82 (2H, quint., $J=7.10$, $\underline{CH_2}CH_2OAr$); 1.64 (3H, d, $J=7.1$, CH_3C^*); 1.20–1.50 (18H, m,CH_2); 0.90 (6H, m, CH_3).

For **IIIa *m/n*** and **IIIb *m/n*** homologues, the general synthetic procedure is shown in scheme 4. The acid **4** was protected by chloroformate in NaOH/water solution with ice cooling. The precipitate, which is only slightly soluble in ethanol or chloroform, was crystallized

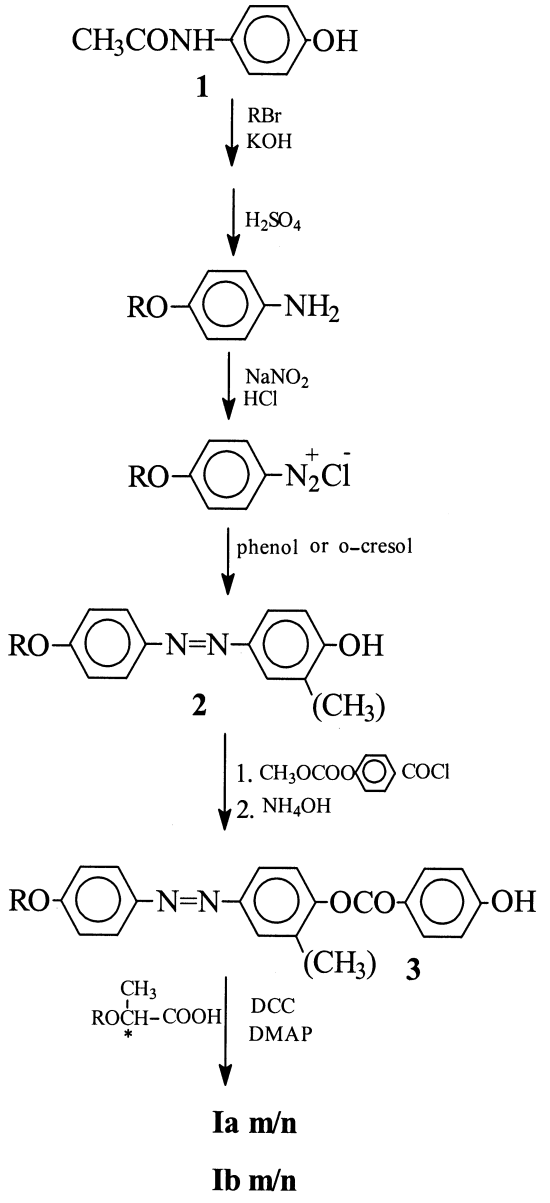

Scheme 2. General procedure for the synthesis of **Ia** ***m/n*** and **Ib** ***m/n*** homologues.

from ethanol/dioxan mixture. The product was converted by thionyl chloride to the acid chloride and after reaction with the appropriate alkyllactate it was deprotected by ammonolysis under standard conditions. The final products **IIIa** ***m/n*** and **IIIb** ***m/n*** were obtained by esterification of **7** with the appropriate 4-alkoxybenzoic acids and 4-alkoxy-3-methylbenzoic acids, respectively, in dichloromethane in the presence of DCC as condensation agent and DMAP as catalyst. ^{1}H NMR ($CDCl_3$, 200 MHz) for **IIIb 8/6** δ (ppm): 8.25 (2H, d, $J=8.4$, *ortho* to –COOCH); 8.17 (2H, d, $J=8.8$, *ortho* to –COOAr); 7.90–8.10 (4H, m, *ortho* to –N=N–); 7.40 (2H, d, $J=8.8$, *ortho* to –OCOAr); 7.00 (2H, d, $J=8.8$, *ortho* to –O*R*); 5.35 (1H, q, $J=6.9$, C*H); 4.20 (2H, t, $J=6.8$, C*H–COO$\underline{CH_2}$); 4.05 (2H, t, $J=6.4$, CH_2OAr); 1.95 (3H,d, $J=6.95$, CH_3 C*); 1.85 (2H, quint., $\underline{CH_2}$ CH_2OAr); 1.20–1.50 (18H, m, CH_2); 0.90 (6H, m, CH_3).

All crude products were purified by column chromatography on silica gel using a mixture of dichloromethane and ethanol (99/1) as an eluant. Structures of all the prepared products were confirmed by ^{1}H NMR spectroscopy. The chemical purity of the compounds was checked by high pressure liquid chromatography (HPLC), which was carried out with an Ecom HPLC chromatograph using a silica gel column (Separon 7 μm, 3 × 150, Tessek) with a mixture of 99.9% of toluene and 0.1% of methanol as eluant; detection of the eluting products was by a UV-Vis detector ($\lambda=290$ nm). The chemical purity of all the synthesized compounds was found to be between 99.6 and 100%.

3. Experimental results

Microscopic observations and measurements of the basic physical characteristics were carried out on planar samples (in the bookshelf geometry) filled in the isotropic phase into 25-μm thick glass cells by means of capillary action. The inner surfaces of the glass plates were covered by ITO electrodes and polyimide layers unidirectionaly rubbed, to ensure planar (bookshelf) alignment. Further improvement of the alignment was achieved by an electric field (10–20 Hz, 40 kV cm^{-1}) applied for about 5–30 min.

3.1. *Mesomorphic properties*

For all the synthesized materials the phase sequences and phase transition temperatures were determined on cooling from the isotropic phase from the observation of characteristic textures and their changes in planar cells when viewed through the polarizing microscope (Nicon Eclipse E600POL). A Linkam LTS E350 heating stage with TMS 93 temperature programmer was used for the temperature control, which enabled temperature stabilization within ± 0.1 K. For some of the materials studied the phase transition temperatures were checked by differential scanning calorimetry (Perkin-Elmer DSC7). Melting points, phase transition temperatures and values of the spontaneous polarization are shown in tables 1, 2 and 3.

Compounds in the **Ia** ***m/n*** series containing the lateral methyl group, and non-substituted **Ib** ***m/n*** homologues with the shortest non-chiral chain (***m*** = **4**) show only the cholesteric phase over a broad temperature range (see table 1). For other non-substituted **Ib** ***m/n*** materials, a broad ferroelectric SmC* phase of about 10–30 K was

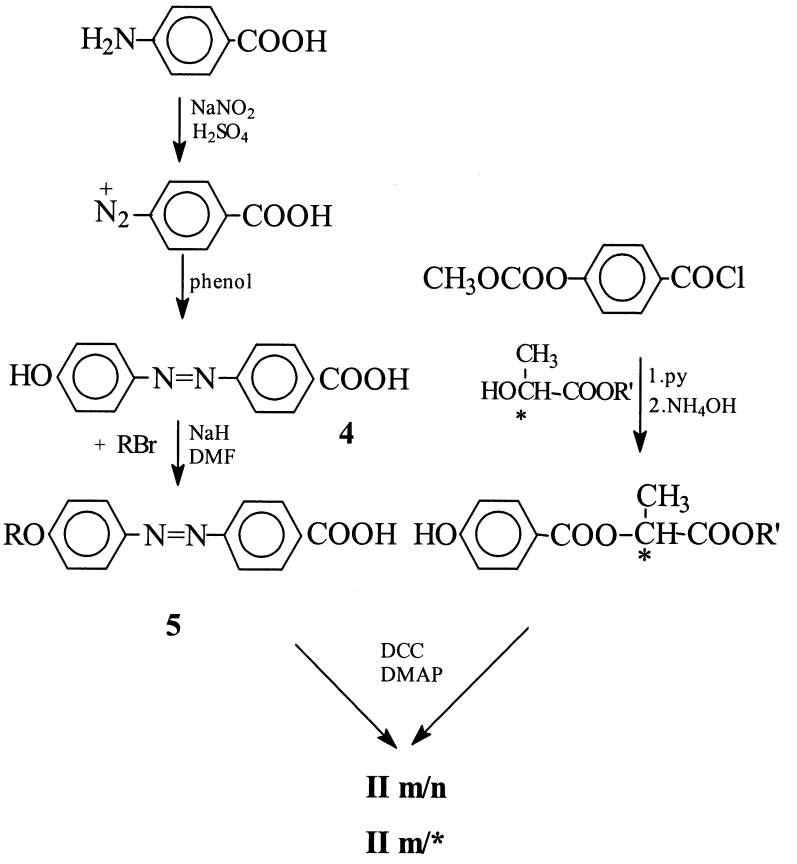

Scheme 3. General procedure for the synthesis of **II** ***m/n*** and **II** ***m/***** homologues.

exhibited below the cholesteric phase. For compounds **II** ***m/**** and **II** ***m/n*** with no substitution, the paraelectric SmA phase appears on cooling from the isotropic phase instead of the cholesteric phase observed for the **I** and **III** series. For **II** ***m/n*** compounds with one chiral centre, the monotropic ferroelectric SmC* phase shifts to lower temperatures compared with that of the **II** ***m/**** materials with two chiral centres. For compound **II 7/10**, the ferroelectric SmC* phase does not appear at all; only the paraelectric SmA phase was observed down to room temperatures. For the methyl-substituted materials from the **IIIa** ***m/n*** series, the blue phase and the cholesteric phase were observed. The cholesteric phase region was more than 70 K down to room temperatures. The non-substituted materials **IIIb 8/6** and **IIIb 10/6** show the blue phase, the cholesteric phase and the paraelectric SmA phase, while **IIIb 7/6** shows the cholesteric phase and a low temperature orthogonal smectic phase, probably the SmB phase.

3.2. *Spontaneous quantities*

In the ferroelectric SmC* phase the temperature dependence of the spontaneous polarization ($\mathbf{P}_s$), the spontaneous tilt angle (θ_s) of the molecules from the smectic layer normal and the helix pitch length (p) have been measured.

3.2.1. *Spontaneous polarization*

Values of the spontaneous polarization have been evaluated from the $\mathbf{P}(E)$ hysteresis loop detected during $\mathbf{P}_s$ switching in an a.c. electric field E of frequency 60 Hz. The temperature dependence of the spontaneous polarization for the non-substituted **Ib** ***m/n*** series is shown in figure 1. At the N*→SmC* phase transition, a finite jump up in $\mathbf{P}_s$ was found, which is typical behaviour for a first-order phase transition. For this series the spontaneous polarization does not saturate, but exhibits a slight continuous increase on cooling. It can be seen from figure 1 that there is a decrease in the $\mathbf{P}_s$ values with increasing the number of the carbon atoms (***n***) in the chiral chain. However, the value of the spontaneous polarization remains almost constant on changing the number of carbons ***m*** in the non-chiral chain.

The temperature dependence of the spontaneous polarization for the non-substituted **II** ***m/n*** and **II** ***m/****

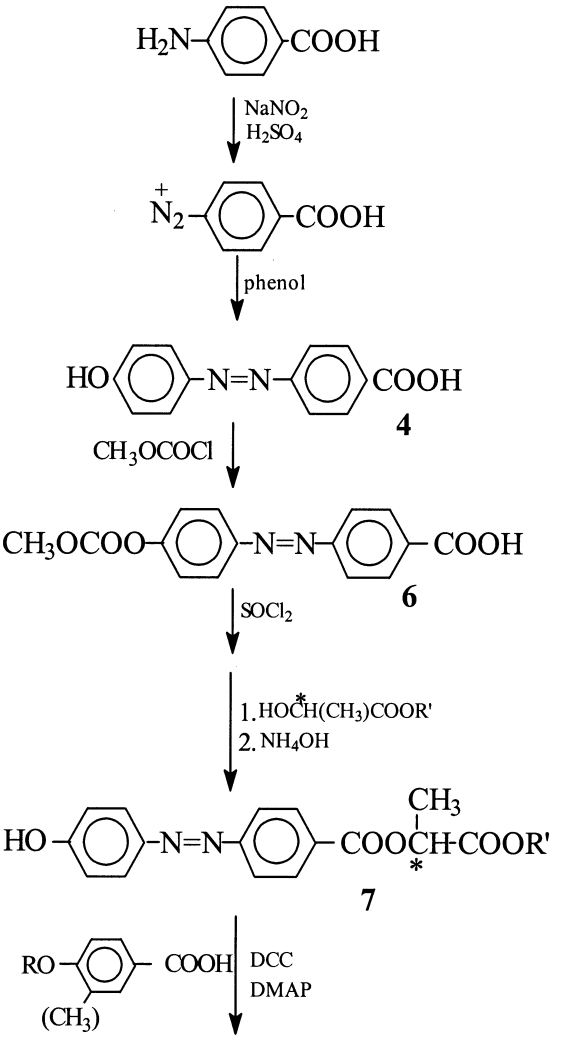

Scheme 4. General procedure for the synthesis of **IIIa** ***m/n*** and **IIIb** ***m/n*** homologues.

series are shown in figure 2. Values of the $\mathbf{P}_s$ increase continuously from zero as the temperature decreases from the SmA→SmC* phase transition. This behaviour is a typical manifestation of a second-order phase transition. The spontaneous polarization does not saturate at low temperatures.

3.2.2. *Spontaneous tilt angle*

The values of the spontaneous tilt angle were determined optically from the difference between the extinction positions viewed between crossed polarizers under opposite d.c. electric fields of $\pm 40\,\mathrm{kV\,cm^{-1}}$. Well aligned samples were used for θ_s measurements. For **Ib** ***m/n*** homologues, the values of the spontaneous tilt angle, being temperature independent, were within the range 38–42° for all these compounds.

The temperature dependence of the spontaneous tilt angle for compounds from the **II** ***m/n*** and **II** ***m/**** series are shown in figure 3. Starting at the SmA→SmC* phase transition temperature, the values of the tilt angle increase continuously from zero reaching a saturation value at the low temperature limit of the ferroelectric phase. For both series, the spontaneous tilt angle is higher for the longer non-chiral chain.

3.2.3. *Helix pitch*

The values of the helix pitch length were established by diffraction of He-Ne laser light (631 nm) on

Table 1. Phase sequences melting points (m.p., °C), phase transition temperatures (°C) measured on cooling (5 K min^{-1}), and values of spontaneous polarization $\mathbf{P}_s$ (nC cm^{-2}) measured at temperatures 10 K below the transition to the SmC* phase, for the **Ia** ***m*/*n*** and **Ib** ***m*/*n*** homologous series.

Compound	*m*	*n*	*X*	m.p.	Cr		SmC*		N*		I	P_s
Ia	**4**	**8**	CH_3	58	•	34	—		•	101	•	—
Ia	**6**	**12**	CH_3	56	•	40	—		•	81	•	—
Ia	**10**	**8**	CH_3	65	•	49	—		•	96	•	—
Ia	**10**	**12**	CH_3	64	•	50	—		•	86	•	—
Ib	**4**	**8**	H	94	•	86	—		•	158	•	—
Ib	**4**	**12**	H	100	•	92	—		•	139	•	—
Ib	**6**	**6**	H	88	•	79	•	101	•	166	•	100
Ib	**6**	**8**	H	92	•	85	•	102	•	153	•	92
Ib	**6**	**10**	H	93	•	86	•	104	•	142	•	86
Ib	**6**	**12**	H	91	•	86	•	96	•	136	•	65
Ib	**8**	**12**	H	93	•	88	•	110	•	133	•	68
Ib	**10**	**5**	H	101	•	91	•	125	•	151	•	86
Ib	**10**	**12**	H	98	•	91	•	121	•	132	•	67

Table 2. Phase sequences melting points (m.p., °C), phase transition temperatures (°C) measured on cooling (5 K min^{-1}), and values of spontaneous polarization $\mathbf{P}_s$ (nC cm^{-2}) measured at temperatures 10 K below the transition to the SmC* phase, for the **II** ***m*/*** and **II** ***m*/*n*** homologous series.

Compound	*m*	*n*	m.p.	Cr		SmC*		SmA		I	P_s
II	**7**	*	89	•	58	•	93	•	155	•	63
II	**10**	*	92	•	75	•	115	•	139	•	68
II	**7**	**6**	70	•	36	•	58	•	159	•	41
II	**8**	**6**	74	•	20	•	66	•	150	•	39
II	**7**	**10**	57	•	34	—		•	142	•	—

Table 3. Phase sequences melting points (m.p., °C), and phase transition temperatures (°C) measured on cooling (5 K min^{-1}), for the **IIIa** ***m*/*n*** and **IIIb** ***m*/*n*** homologous series.

Compound	*m*	*n*	*X*	m.p.	Cr		SmA		N*		BP		I
IIIa	**7**	**6**	CH_3	49	•	20	—		•	105	•	106	•
IIIa	**8**	**6**	CH_3	59	•	31	—		•	101	•	102	•
IIIa	**10**	**6**	CH_3	45	•	24	—		•	93	•	95	•
IIIb	**7**	**6**	H	65	•	68	[a]	132	•	162	—		•
IIIb	**8**	**6**	H	75	•	47	•	128	•	138	•	140	•
IIIb	**10**	**6**	H	63	•	45	•	127	•	130	•	131	•

[a]The SmB phase occurs here.

disclination lines, that exist in planar samples due to the strong polar anchoring at the surfaces (dechiralization lines); the line spacing
equals p.

For **Ib** ***m*/*n*** compounds, the temperature dependence of the helix pitch is shown in figure 4. One can see a strong increase in p on increasing the length of the chiral chain. The value of p was not measured for **Ib 10/5** as the helix remains unwound over the whole temperature range of the SmC* phase. The homologues with the longest chiral chain ($n=12$) exhibit a remarkable temperature dependence of the helix pitch. The highest values are found below the N*→SmC* phase transition. For **II** ***m*/*** and **II** ***m*/*n*** homologues, the values of p could not be

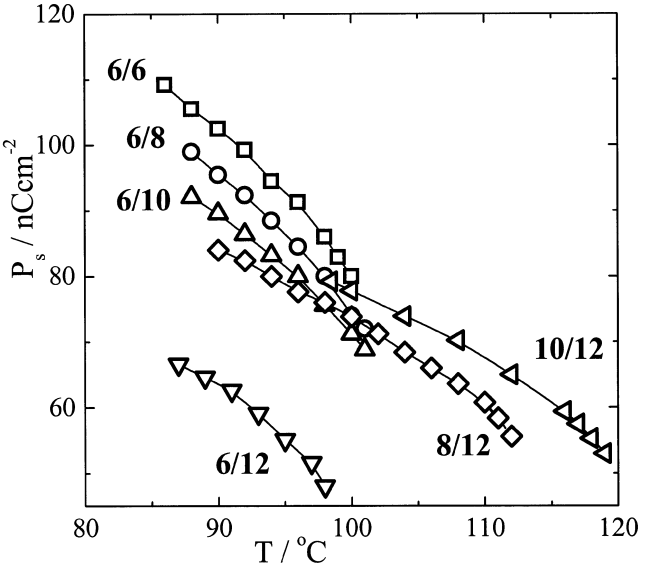

Figure 1. Temperature dependence of the spontaneous polarization $\mathbf{P}_s(T)$ for the **Ib 6/*n*** and **Ib *m*/12** sub-series.

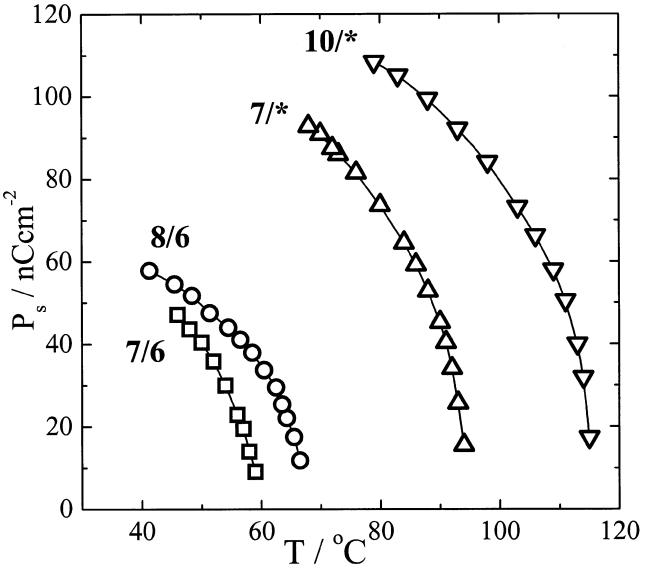

Figure 2. Temperature dependence of the spontaneous polarization $\mathbf{P}_s(T)$ for the **II** ***m*/*** and **II** ***m*/*n*** series.

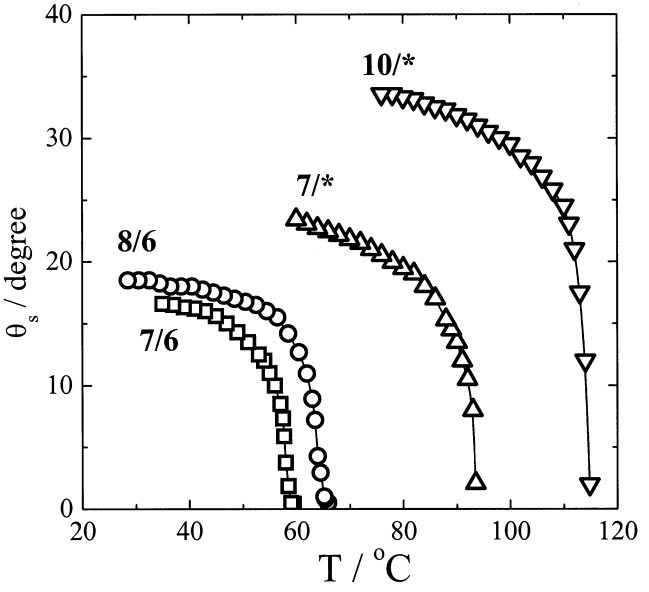

Figure 3. Temperature dependence of the spontaneous tilt angle $\theta_s(T)$ for the **II *m*/*** and II ***m*/*n*** series.

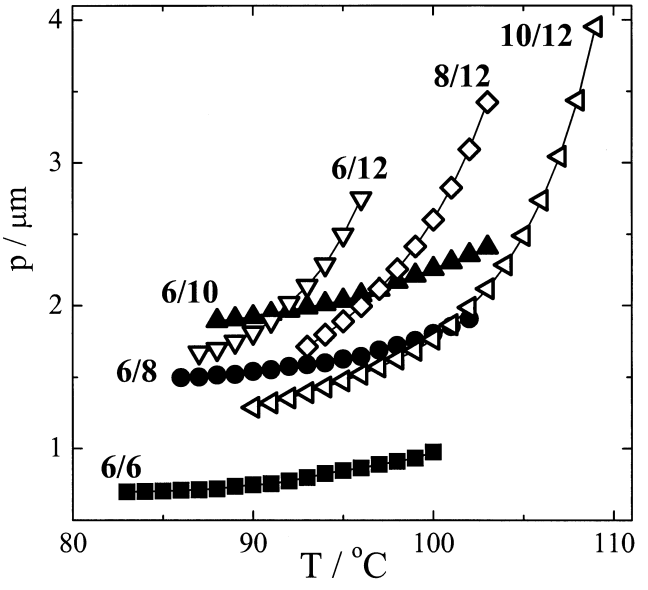

Figure 4. Temperature dependence of the helix pitch length, p(T), for the **Ib *m*/*n*** series.

measured as the dechiralization line spacing was rather large and irregular, which means that the helix remains almost unwound over the temperature range of the SmC* phase.

3.3. *Dielectric properties*

A Schlumberger 1260 impedance analyser was used for the dielectric measurements. The temperature

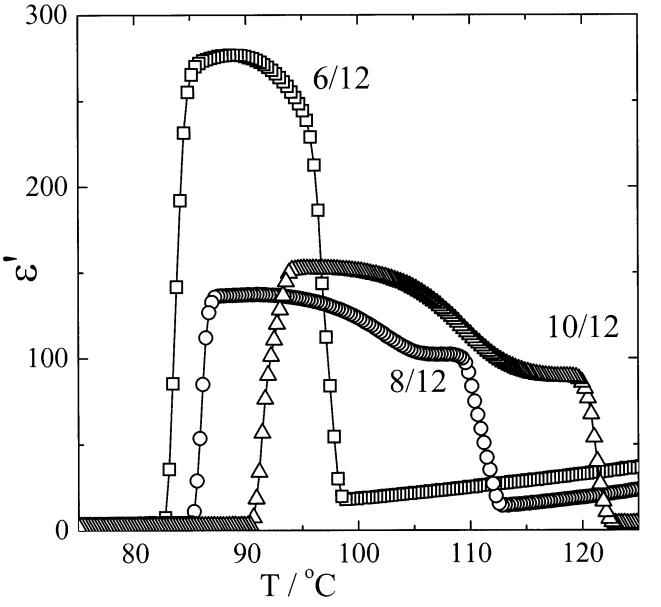

Figure 5. Temperature dependence of the real part $\varepsilon'(T)$ of the complex permittivity for indicated compounds from the **Ib *m*/*n*** series measured on cooling at a frequency of 100 Hz.

dependence of the real part (ε') of the complex permittivity ($\varepsilon^* = \varepsilon' - i\varepsilon''$) has been measured on cooling for the compounds studied at a frequency of 100 Hz. For the non-substituted **Ib *m*/12** series, the temperature dependence of the real part of the complex permittivity is shown in figure 5. There is a great increase of permittivity in the SmC* phase due to the contribution of the Goldstone mode. Qualitatively, the same results have been obtained for the **II m/*n*** and **II *m*/*** series.

For all the materials, the frequency dispersions of the complex permittivity have been measured on cooling in the frequency range of 1 Hz–1 MHz, keeping the temperature stable during the frequency sweep to within ± 0.1 K. The frequency dispersion data were analysed within the temperature range of the SmA and SmC* phases using the Cole–Cole formula for the frequency-dependent complex permittivity:

$$\varepsilon^* - \varepsilon_\infty = \frac{\Delta\varepsilon}{1 + (if/f_r)^{(1-\alpha)}} - i\frac{\sigma}{2\pi\varepsilon_0 f^n}$$

where f_r is the relaxation frequency, $\Delta\varepsilon$ is the dielectric strength, α is the distribution parameter, ε_o is the permittivity of a vacuum, ε_∞ is the high frequency permittivity and n is the parameter of fitting. The second term in the equation is used to eliminate the low frequency contribution to ε'' from d.c. conductivity, σ.

For **Ib *m*/*n*** compounds, it was impossible to eliminate the contribution of the Goldstone mode in the ferroelectric SmC* phase from an extremely strong

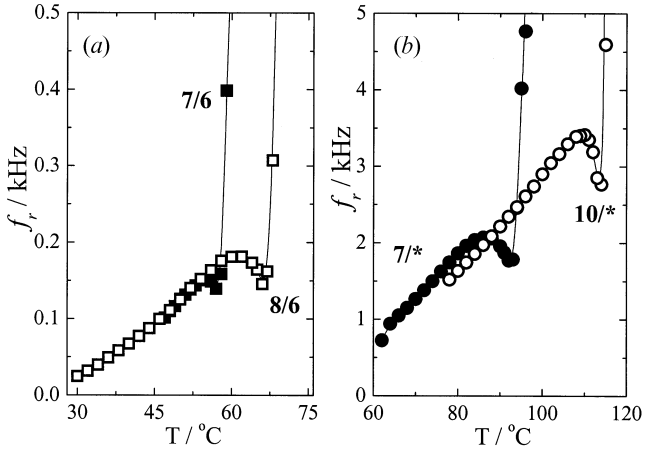

Figure 6. Temperature dependence of the relaxation frequency $f_r(T)$ of the soft (in the paraelectric SmA phase) and Goldstone (in the ferroelectric SmC* phase) modes for indicated compounds from the (*a*) **II *m*/*** and (***b***) **II *m*/*n*** series.

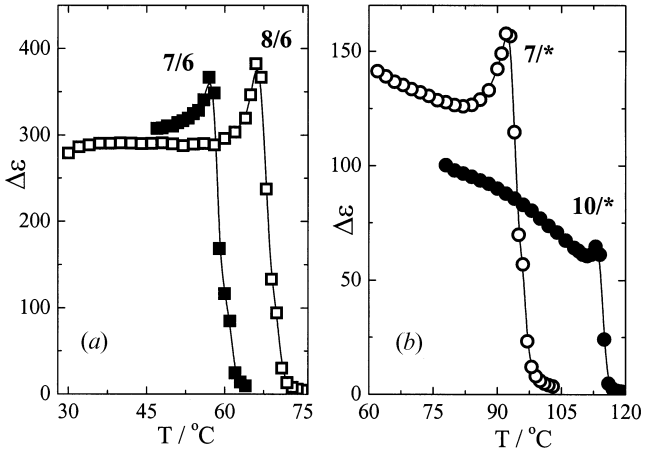

Figure 7. Temperature dependence of the dielectric strength $\Delta\varepsilon(T)$ of the soft and Goldstone modes for indicated compounds from the (*a*) **II *m*/*** and (***b***) II ***m*/*n*** series.

conductivity contribution up to tens of kHz. For **II *m*/*** and **II *m*/*n*** compounds, the dielectric strength and relaxation frequency of the soft and Goldstone modes are shown in figures 6 and 7, respectively. In the SmA phase, the frequency of the soft mode decreases linearly and the dielectric strength increases steeply when approaching the transition temperature to the ferroelectric SmC* phase, where the main contribution to the dielectric permittivity is due to the Goldstone mode. For **II *m*/*n*** compounds the relaxation frequency of the Goldstone mode, being between 50–200 Hz, is about one-tenth that for **II *m*/*** compounds, while the dielectric strength of the mode for **II *m*/*n*** is about three times that for **II *m*/*** compounds.

4. Discussion and conclusions

Six new series of ferroelectric liquid crystalline materials containing an azo group in different positions of the core unit and with or without methyl substitution were synthesized and studied. Alkoxypropionate or alkyllactate units were used as the chiral segments of these materials.

The non-substituted **Ib *m*/*n*** homologues exhibit the N* and SmC* phases, each over a very broad temperature range. In compounds **Ib 4/8** and **Ib 4/12** with the shortest non-chiral chain, the ferroelectric SmC* phase does not appear. The same behaviour was observed for similar compounds in which the ester group is present instead of the azo group [17].

In non-substituted **II *m*/*** and **II *m*/*n*** compounds, the paraelectric SmA phase appears instead of the N* phase observed for the substituted **Ia *m*/*n*** and **IIIa *m*/*n*** series. In the substituted **Ia *m*/*n*** and **IIIa *m*/*n*** series no smectic phase is present. In **II *m*/*n*** homologues, the ferroelectric SmC* phase shifts to lower temperatures with respect to those seen for the **II *m*/*** series where two asymmetric carbon atoms are used in the chiral chain. In compound **II 7/10**, no ferroelectric SmC* phase appears.

The lateral methyl group substituent (series **Ia *m*/*n*** and **IIIa *m*/*n***) probably causes steric hindrance, which inhibits the parallel arrangement of the molecules in the SmC* and SmA layers. Thus, cholesteric ordering is preferred for this type of molecule. This steric hindrance also causes a decrease of all the phase transition temperatures compared to the non-substituted compounds from series **Ib *m*/*n*** and **IIIb *m*/*n***.

Compounds **Ib 8/12** and **Ib 10/12** can be compared to similar materials having the same lateral chains, but carboxy [18] or ester [19] groups instead of the azo group in the core. For those compounds, which have similar distributions of electron density in the molecule, the same phase sequences and similar phase transition temperatures were observed.

For compounds from the **Ib *m*/*n*** series, the values of spontaneous polarization decrease with increasing number of the carbon atoms ***n*** in the chiral chain, but remain nearly constant on changing the number of carbon atoms ***m*** in the non-chiral chain. Increasing the number of carbon atoms in the chiral chain increases the pitch length.

For **II *m*/*** and **II *m*/*n*** compounds, θ_s as well as $\mathbf{P}_s$ increase continuously from zero, when the temperature decreases from the SmA→SmC* phase transition, which is typical for a second-order phase transition. In addition, **II *m*/*** homologues have higher values of $\mathbf{P}_s$ than **II *m*/*n*** homologues, reaching values of about $100\,\mathrm{nC\,cm^{-2}}$.

The results of dielectric spectroscopy for the **II *m*/*n***

and **II** ***m*/*** series show that the relaxation frequency of the soft mode in the SmA phase decreases linearly when approaching the SmA→SmC* phase transition temperature. In the SmC* phase, the Goldstone mode contributes to the permittivity except in the vicinity of the phase transition, where the Goldstone mode may be mixed with the weak soft mode. The coexistence of both modes is indicated by the increase of the parameter α to 0.25. The Goldstone mode properties, namely, the relaxation frequency and the dielectric strength, depend on the helix pitch length p, on the twist elastic constant K and on the viscosity γ [20, 21] as $f_G = 4\pi^2 K/\gamma p^2$ and $\Delta\varepsilon_G \approx (1/8\pi^2 K)(pP_s/\theta_s)^2$, respectively. For the materials from the **II** ***m*/*n*** and **II** ***m*/*** series, the decrease of the relaxation frequency f_r on cooling may be explained by the increase of the viscosity as the helix pitch remains nearly unwound over the whole temperature range of the SmC* phase. For the **II** ***m*/*** series, the increase of the dielectric strength $\Delta\varepsilon$ (except in the vicinity of the phase transition to the SmC* phase) may be explained by the gradual increase of the ratio P_s/θ_s on cooling (see figures 2 and 3). A higher elastic constant can increase the relaxation frequency and lower the dielectric strength in compounds from the **II** ***m*/*** series compared with the **II** ***m*/*n*** series.

For the non-substituted compounds, the position of the azo group located between the first and second aromatic rings of the mesogen (series **Ib** ***m*/*n*** and **II** ***m*/*n***), probably does not influence the stability of the SmC* phase significantly. The ferroelectric phase completely disappears, if the azo group is placed closer to the chiral centre (series **IIIa** ***m*/*n*** and **IIIb** ***m*/*n***). This may be caused by changes of electron density in the mesogenic part of the molecule. While the **II** ***m*/*n*** and **II** ***m*/*** series have the lowest electron densities on the central aromatic ring, the **IIIa** ***m*/*n*** and **IIIb** ***m*/*n*** compounds have the highest deficit of π-electrons on the ring closest to the chiral centre. In this way the value of the dipole moment of the carbonyl group in the chiral unit is decreased and the effect of the chiral unit on the transverse dipole moment of the molecule is weakened, which might suppress the ferroelectric phase. Kaspar *et al*. [17] have studied a series of materials similar to **IIIa** ***m*/*n*** and **IIIb** ***m*/*n***, but with the azo group replaced by the ester group. In these, the deficiency of electrons on the phenyl ring closest to the chiral centre is suppressed by the mesomeric effect of non-bonding orbitals of the oxygen atom which can increase the transverse dipole moment. Due to this effect the ferroelectric SmC* phase may be expected in materials with the ester group in the core.

The compounds with the azo group in the molecule core have very good thermal stability (much higher than Schiff's bases with imine groups in the molecule). In addition, these materials are very interesting for the study of photoisomerization and photoconductivity in liquid crystals. In the solid phase, only the *trans*-isomer is present; generally, in solution or in the liquid crystalline state the *cis*-isomer is produced under illumination by 300–400 nm UV light. The *cis*/*trans* ratio of the isomers can be easily determined by high pressure liquid chromatography.

It is known that the bent *cis*-isomers can pack less easily into layers than linear-shaped *trans*-isomers, which leads to the destruction of mesophases [22]. With the compounds studied, *trans*/*cis*-isomerization has been observed in solution under daylight. In the liquid crystalline state no changes in the properties studied have been found during the experiments nor under microscopic observation. *Trans*/*cis*-isomerization occurs easily in liquid crystals with banana-shaped molecules having an azo group in both arms. Under illumination during microscopy observations, the mesophases have been gradually destroyed [23]. Detailed studies of this phenomenon are now in progress.

This work was supported by Grants No. 202/03/P011 and 202/02/0840 from the Grant Agency of the Czech Republic, Research Project AVOZ1-010-914 and European Project COST D014 WG00015.

References

[1] Ruslim, CH., and Ichimura, K., 1999, *J. Mater. Chem.*, **9,** 673.
[2] Belmar, J., Parra, M., Zuniga, C., Perez, C., Munoz, C., Omenat, A., and Serrano, J. L., 1999, *Liq. Cryst.*, **26,** 389.
[3] Lai, L. L., Wang, E., Liu, Y. H., and Wang, Y., 2002, *Liq. Cryst.*, **29,** 871.
[4] Prajapati, A. K., 2001, *Mol. Cryst. liq. Cryst.*, **364,** 769.
[5] Komitov, L., Ichimura, K., and Strigazzi, A., 2000, *Liq. Cryst.*, **27,** 51.
[6] Komitov, L., Ruslim, C., Matsuzawa, Y., and Ichimura, K., 2000, *Liq. Cryst.*, **27,** 1011.
[7] Kong, B., Bui, L., Xie, P., Zhang, R. B., He, CH., and Chung, N., 2000, *Liq. Cryst.*, **27,** 1683.
[8] Tang, Y. X., Xie, P., Liu, D. S., and Zhang, R. B., 1997, *Macromol. Chem. Phys.*, **198,** 1855.
[9] Tian, Y., Ren, Y., Sun, R., Zhao, Y., Tang, X., Huang, X., and Xi, S., 1997, *Liq. Cryst.*, **22,** 177.
[10] Shirota, K., Yamaguchi, I., Kanie, K., Ikeda, T., Hiyama, T., Kobayashi, I., and Suzuki, Y., 2000, *Liq. Cryst.*, **27,** 555.
[11] Negishi, M., Kanie, K., Ikeda, T., and Hiama, T., 1996, *Chem. Lett.*, **8,** 583.
[12] Werth, M., Nguyen, H. T., Destrade, C., and Isaert, N., 1994, *Liq. Cryst.*, **17,** 863.
[13] Shereshovets, N. N., Komyak, A. I., and Minko, A. A., 1981, in Abstracts of the 4th Liquid Crystal

Conference of Socialist Countries, Tbilisi, USSR, Abstract No. F62.
[14] XU, Z., LEMIEUX, R. P., NATANSOHN, A., ROCHON, P., and SHASHIDHAR, R., 1999, *Liq. Cryst.*, **26,** 351.
[15] KAŠPAR, M., HAMPLOVÁ, V., PAKHOMOV, S. A., STIBOR, I., SVERENYÁK, H., BUBNOV, A. M., GLOGAROVÁ, M., and VANĚK, P., 1997, *Liq. Cryst.*, **22,** 557.
[16] WOLFF, D., CACKOVIC, H., KRUGER, H., RUBNER, J., and SPRINGER, J., 1993, *Liq. Cryst.*, **14,** 917.
[17] KAŠPAR, M., HAMPLOVÁ, V., PAKHOMOV, S. A., BUBNOV, A. M., GUITTARD, F., SVERENYÁK, H., STIBOR, I., VANĚK, P., and GLOGAROVÁ, M., 1998, *Liq. Cryst.*, **24,** 599.
[18] PAKHOMOV, S. A., KAŠPAR, M., HAMPLOVÁ, V., BUBNOV, A. M., SVERENYÁK, H., GLOGAROVÁ, M., and STIBOR, I., 1998, *Ferroelectrics*, **212,** 341.
[19] VAJDA, A., KAŠPAR, M., HAMPLOVÁ, V., VANĚK, P., BUBNOV, A., FODOR-CSORBA, K., and EBER, N., 2001, *Mol. Cryst. liq. Cryst.*, **365,** 569.
[20] BLINC, R., and Žekš, B., 1978, *Phys. Rev. A*, **18,** 740.
[21] CARLSSON, T., Žekš, B., FILIPIČ, C., LEVSTIK, A., and BLINC, R., 1988, *Mol. Cryst. liq. Cryst.*, **163,** 11.
[22] DEMIKHOV, E. I., JOHN, M., and KROHN, K., 1997, *Liq. Cryst.*, **23,** 443.
[23] BUBNOV, A., KAŠPAR, M., HAMPLOVÁ, V., and GLOGAROVÁ, M., 2003, presented at the 9th International Conference on FLC, Dublin, Ireland, poster P-092.